RSC Advances

ROYAL SOCIETY OF CHEMISTRY

www.rsc.org/advances

Journal Name

ARTICLE

Mechanism of short-pulse-induced solute migration in comparison to continuous-light-driven thermal diffusion

Received 00th January 20xx,
Accepted 00th January 20xx

DOI: 10.1039/x0xx00000x

www.rsc.org/

Li-Shu Lee,[a] Yu-Ting Kuo,[a] Chi-Chen Wang,[a] Yi-Ci Li,[a] Po-Yuan Huang,[a] Cheng-I Lee[b, †] and Tai-Huei Wei[a, †]

The aim of this work is to clarify the mechanism of photo-absorption-caused solute migration at the microscopic level. Experimentally, we respectively measured the short-pulse-induced and continuous-light-driven migrations of chloroaluminum phthalocyanine molecules dissolved in ethanol at two concentrations, 4.2×10^{17} cm^{-3} (7.0×10^{-4} M) and 1.2×10^{17} cm^{-3} (2.0×10^{-4} M). Theoretically, by verifying that individual solute molecules in the concentrated solution, compared to those in the dilute solution, absorb more photo energy collectively but less photo energy individually, we consider solute migration as net movement of individual solute molecules and then sequentially analyse how individual solute molecules absorb photo energy, convert the absorbed photo energy into translational excess energy intra-molecularly and carry out movement. Subsequently, by summing up movement of individual solute molecules in a unit of volume, we deduce the solute migration behaviours which coincide with the experimental results: for short pulse excitation, solute migration is more/less in the concentrated solution depending on the pulse energy; for continuous light irradiation, solute migration is always more in the concentrated solution regardless of the light power. Note that, in our theoretical deduction, the short-pulse-induced and continuous-light-driven solute migrations differ in that the former proceeds before inter-molecular relaxation becomes apparent and the latter carries on with inter-molecular relaxation practiced sufficiently. Accordingly, the former is non-quasistatic and the latter is quasistatic and thus referred to as thermal diffusion.

1. Introduction

When a multicomponent fluid is in full thermodynamic (thermal, mechanical and chemical) equilibrium, each constituent molecule is confined within a Lennard-Jones potential well (Fig. 1) formed by the attractive forces of neighbouring molecules.[1] After individual molecules of a specific component are supplied with excess energy $\Delta\varepsilon_e$ and a fraction of this $\Delta\varepsilon_e$ is converted into translational excess energy $\Delta\varepsilon_t$ intra-molecularly, they may move toward molecules of the same component that are supplied with less $\Delta\varepsilon_e$ individually. Depending on the composite time rate of $\Delta\varepsilon_e$ supply and intra-molecular $\Delta\varepsilon_e$ into $\Delta\varepsilon_t$ conversion relative to that of inter-molecular excess energy transfer, individual molecules of the specific component may move in drastically different ways. Correspondingly, the specific component shows different behaviours of molecular migration, net movement of individual molecules in a unit of volume.

Undoubtedly, thermal diffusion is the most widely known molecular migration process. It pertains to the situation that the composite time rate of $\Delta\varepsilon_e$ supply to individual molecules of a specific component and intra-molecular $\Delta\varepsilon_e$ into $\Delta\varepsilon_t$ conversion is much lower than that of inter-molecular excess energy transfer. Accordingly, during the $\Delta\varepsilon_e$ supply and $\Delta\varepsilon_e$ into $\Delta\varepsilon_t$ conversion, nearly equal $\Delta\varepsilon_t$ is gathered in neighbouring individual molecules of all the other components via inter-molecular energy transfer. This signifies that individual molecules of all the components inevitably move synchronously in response to the supplying of $\Delta\varepsilon_e$ to individual molecules of the specific component. In the process of movement, individual molecules of all the components stay confined in the Lennard-Jones potential wells, with the well shapes distorted from the ones pertaining to the fluid in full thermodynamic equilibrium. This is because individual molecules of each component in the same volume element dV do not necessarily move at the same velocity due to the difference in molecular weight of each component and the inter-molecular interaction. Hence, the spatial distribution of molecules of all the components changes in the meantime. Moreover, because inter-molecular energy transfer is sufficiently practiced with movement of

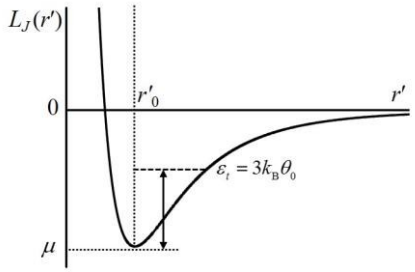

Fig. 1 The Lennard-Jones potential well for translation (oscillation) of an individual molecule. L_J denotes the potential energy, $r'–r'_0$ the distance between the molecule and its equilibrium position, μ (<0) the minimum of L_J, ε_t the translational energy and k_B the Boltzmann constant. At room temperature θ_0=298 K, the molecule is confined within the well.

[a] Department of Physics, National Chung Cheng University, Min-Hsiung, Chia-Yi 621, Taiwan.
[b] Department of Life Science, National Chung Cheng University, Min-Hsiung, Chia-Yi 621, Taiwan.
† Corresponding author: 886-5-272-0411 ext. 66324; E-mail address: twei@ccu.edu.tw. 886-5-272-0411 ext. 66511; E-mail address: biocil@ccu.edu.tw.
Electronic Supplementary Information (ESI) available: [details of any supplementary information available should be included here]. See DOI:10.1039/x0xx00000x

individual molecules, the fluid deviates infinitesimally from local thermodynamic equilibrium. Thus, molecular migration of the specific component with all the other components is a quasistatic process. Note that when the fluid is in local thermodynamic equilibrium, ε_t ($\equiv\varepsilon_{t0}+\Delta\varepsilon_t$, with ε_{t0} being the translational energy of individual molecules of each component given the fluid in full thermodynamic equilibrium) is nearly equal for individual molecules of all the components contained in the same dV. Hence, the solution temperature θ pertaining to this dV is definable and may differ slightly from that of a neighbouring dV. According to the equipartition theorem, θ is proportional to $<\varepsilon_t>$, the average of ε_t over all the molecules contained in the same dV, given the sample in (full or local) thermodynamic equilibrium.[2] Therefore, when the driving forces of molecular migrations of the specific component and all the other components, measured in the center of mass coordinate, are proportional to the gradient of $<\varepsilon_t>$ ($\nabla<\varepsilon_t>$), they are indeed proportional to $\nabla\theta$.[3] Here, the factor of the proportionality may be θ ($\propto<\varepsilon_t>$) dependent.[4]

Thermal diffusion has been widely studied in various types of chemical systems, including liquid mixtures,[5] aerosol mixtures,[6] polymer solutions,[7,8] colloidal suspensions,[9–11] nanoparticles,[12] nucleotides,[13] and magnetic fluids.[14–16] Recently, the measurement of infrared-irradiation-induced thermal diffusion has been developed into a powerful assay for basic and translational research, as well as for drug discovery.[17]

Considering a scenario that the composite time rate of $\Delta\varepsilon_e$ supply to individual molecules of a specific component and intra-molecular $\Delta\varepsilon_e$ into $\Delta\varepsilon_t$ conversion is larger or comparable to that of inter-molecular excess energy transfer, we wonder whether the resultant molecular migration of the specific component follows the behaviour of thermal diffusion. When intra-molecular $\Delta\varepsilon_t$ accumulation makes ε_t ($\equiv\varepsilon_{t0}+\Delta\varepsilon_t$) exceed the barrier energy $-\mu$ of the potential well before inter-molecular excess energy becomes apparent, individual molecules of the specific component may acutely escape from the potential well entrapment and move away from their neighbouring molecules, which are standing still with $\varepsilon_t=\varepsilon_{t0}$. Hence, the fluid is not in local thermodynamic equilibrium when the specific component carries out a molecular migration. This signifies that this molecular migration is non-quasistatic. Note that although individual molecules of other components do not move synchronously with those of the specific component, they eventually do after gaining $\Delta\varepsilon_t$ from the specific component that are undergoing migration. Consequently, this migration differs from thermal diffusion.

To explore the non-quasistatic molecular migration in comparison to the quasistatic one, in this study, we used chloroaluminum (ClAl) phthalocyanine (Pc) ($C_{32}H_{16}AlClN_8$) dissolved in ethanol, dubbed ClAlPc/EtOH, as an example of a bicomponent liquid. By preparing this solution at two concentrations, 4.2×10^{17} cm^{-3} (7.0×10^{-4} M) and 1.2×10^{17} cm^{-3} (2.0×10^{-4} M), we respectively conducted the Z-scan measurements, with TEM_{00} mode 19 picoseconds (ps) laser pulses at 532 nm, and the transmittance measurements, with TEM_{00} mode continuous HeNe laser light at 632.8 nm, on this solution. As a result, we find that the concentrated solution shows stronger absorption but more/less solute migration in response to 19 ps pulse excitation, depending on the pulse energy. On the contrary, it always shows stronger absorption and more solute migration in response to continuous light irradiation. To explain the experimental results, we theoretically analyse how individual solute molecules absorb photo energy, convert the absorbed photo energy into translational excess energy intra-molecularly and then carry out movement. Subsequently, we sum up movement of individual solute molecules in a unit of volume to deduce the solute migration behaviours to be compared with the experimental results. A key issue in our analysis lies in the influence of inter-molecular relaxation on the intra-molecular relaxation.

2. Experimental details

In this section, we introduce the Z-scan technique used to investigate the 19-ps-pulse-induced solute migration in ClAlPc/EtOH and the transmittance measurement technique used to explore the continuous-light-driven thermal diffusion in the same solution.

Z-scan technique

Fig. 2(a) shows the Z-scan apparatus.[18] Briefly, a shutter is placed before the beam splitter (BS) in the light path to select pulses at time intervals of any integral multiple of 0.1 s. This makes the pulse-to-pulse separation of $\tau_{p\text{-}p}=h\times0.1$ s, with h denoting any positive integer and 0.1 s being the reciprocal of the repetition rate of the 10 Hz laser. A small portion of an incident laser pulse propagating along the $+z$ axis is directed by the BS to photo-detector D1 that monitors the fluctuation in input pulse energy $\mathcal{E}_1$. The major portion of a pulse passing through the BS is tightly focused to the waist at z=0. The energy $\mathcal{E}_2$ of each pulse transmitted through the sample with its front surface at a certain position z relative to the beam waist is detected by photo-detector D2.

In a Z-scan measurement, the sample is stepped along the $+z$ direction across the beam waist in 0.4 mm increments. The outputs of D1 and D2 for 5 laser pulses are recorded at each sample position z. When the sample travels between two adjacent z positions in less than 1.0 s, we neither deliberately block the laser beam nor perform any measurements. Because the laser tends to fluctuate from pulse to pulse, the recorded D2 output for each laser pulse is divided by the corresponding D1 output to correct for the laser energy fluctuation. The D2/D1 ratio averaged over 5 laser pulses at each z, after being normalized with those at large $|z|$, where the incident intensity is low and thus linear response prevails, is named the normalized transmittance and denoted by NT. A plot of NT as a function of z is named the Z-scan curve.

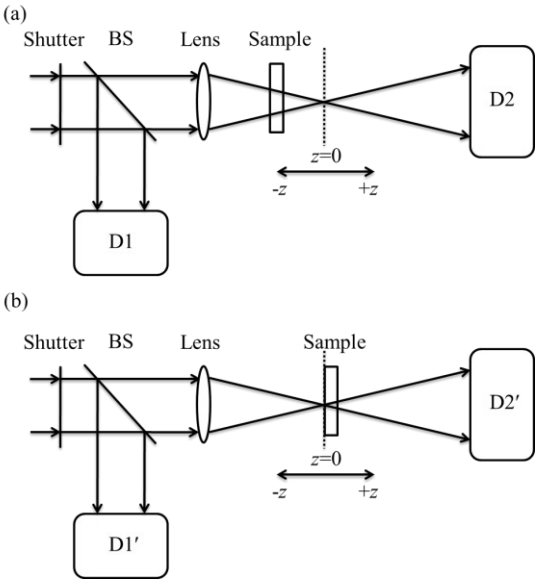

Fig. 2 (a) The Z-scan experimental apparatus that records the transmittance (D2/D1) as a function of the sample's front surface position z. (b) The transmittance measurement technique that records the transmittance (D2′/D1′) as a function of time t with the sample's front surface placed at the beam waist.

The laser used with this technique is a frequency-doubled, Q-switched and mode-locked Nd:YAG laser operating in the TEM_{00} mode and running at 10 Hz with a width of τ=19 ps, measured at half-

width at e^{-1} maximum (HWe^{-1}M). Each output pulse is focused to the waist with radius $w_0 \equiv w(0)$=18.5 μm half-width at e^{-2} maximum (HWe^{-2}M). The mass diffusion time constant τ_{md} for ClAlPc/EtOH at the beam waist is hence estimated, in the manner described in Ref.[19], to be 0.3 s, longer than the shortest available $\tau_{p\text{-}p}$ of 0.1 s. This enables us to tune $\tau_{p\text{-}p}$ across τ_{md}.

The intensity of each pulse incident on the sample′s front surface at z can be written as[20]

$$I_z(r,t) = \left[\frac{w_0^2}{w^2(z)}\right] \times I_{00} \times \exp\left[-\frac{2r^2}{w^2(z)}\right] \times \exp\left(-\frac{t^2}{\tau^2}\right). \quad (1)$$

Here, t and r refer to the temporal and lateral distributions of each pulse. $w(z)=w_0\times[1+(z/z_0)^2]^{1/2}$ is the beam radius (HWe^{-2}M) at z. $z_0 = kw_0^2/2$ is the diffraction length of the beam. $k=2\pi/\lambda$ (λ=532 nm) is the wave propagation number. I_{00} is the on- axis peak intensity at the beam waist. All these parameters pertain to free space. Integration of eqn (1) over t (from $-\infty$ to $+\infty$) and over the whole beam cross section relates I_{00} to $\mathcal{E}_1$ as

$$I_{00} = \frac{2\mathcal{E}_1}{\pi^{3/2} \times w_0^2 \times \tau}. \quad (2)$$

Using pulses at three energy levels, 1.1, 4.5, and 8.7 μJ, we conducted, at room temperature (θ_0=298 K), Z-scan measurements on ClAlPc/EtOH prepared at 4.2×10^{17} cm^{-3} and 1.2×10^{17} cm^{-3} and contained in quartz cuvettes with a thickness of L=1.0 mm.

Although we have considered that a pulse extends temporally from $-\infty$ to ∞ in the derivation of eqn (2), we ignore the pulse for the time beyond $\pm3\tau$ ($\pm$57 ps) when simulating the pulse-matter interaction in the following. This is because the intensity outside the range $[-3\tau, 3\tau]$ is vanishingly small.

Transmittance measurement technique

Fig. 2(b) shows the experimental apparatus for the transmittance measurement technique. To minimize the convection effect, the laser beam propagation direction (+z) is adjusted to point downward to the optical table normally.[21] A shutter is placed before the BS in the light path. A small portion of the incident laser beam is directed by the BS to photo-detector D1′, which monitors the fluctuation in input power P1. The major portion of the laser beam is tightly focused to the waist at z=0. Photo-detector D2′ is placed after the sample, with its front surface at z=0, to record the transmitted power P2. To correct for the laser power fluctuation, the recorded D2′ reading is divided by the corresponding D1′ reading to yield the transmittance (D2′/D1′, denoted by T').

The laser used with this technique is a TEM$_{00}$ mode CW HeNe laser at 632.8 nm. The laser beam radius at the waist is w'_0=19 μm (HWe^{-2}M) and the intensity therein is[20]

$$I'_z(r,t) = I'_{00} \times \exp\left(-\frac{2r^2}{w_0'^2}\right) \times \mathrm{step}(t). \quad (3)$$

Here, t and r refer to the temporal and lateral distributions of the incident laser beam. t=0 denotes the shutter opening time before which the laser beam is blocked to ensure that the sample is in thermodynamic equilibrium with θ_0=298 K. step(t) equals 0 for t<0, 0.5 for t=0 and 1 for t>0. I'_{00} is the on-axis intensity at the beam waist. All these parameters pertain to free space. Integration of eqn (3) over the whole beam cross section relates I'_{00} to P1 as

$$I'_{00} = \frac{2P1}{\pi w_0'^2}. \quad (4)$$

By setting P1 to be 2.5 mW (I'_{00}=440.9 W/cm^2 accordingly), we measured T' of the same sample used in the Z-scan measurements as a function of t.

3. Theory

It is most appropriate to use the five-energy-band (S_0, S_1, S_2, T_1 and T_2) model shown in Fig. 3 to interpret the optical excitation and the subsequent relaxation of ClAlPc/EtOH.[22,23] Each band in Fig. 3, including the associated zero-point level |0) and vibrational levels |v≠0), is conventionally named S_m for the singlet manifold and T_m for the triplet manifold where the subscript m refers to the state formed from certain electronic configurations in molecular orbitals. In full thermodynamic equilibrium, all the ClAlPc molecules reside on S_0. Pumped by a 19 ps pulse at 532 nm, some of them are promoted to $|\nu)S_1$ by one-photon $S_0 \rightarrow |\nu)S_1$ excitation or to $|\nu)S_2$ by two-photon $S_0 \rightarrow |\nu)S_2$ excitation.[24] Those excited to $|\nu)S_1$ first relax to $|0)S_1$ in a sub-ps time frame[25] and then undergo one of the following three processes: (i) fluorescent relaxation to S_0 ($|0)S_1 \rightsquigarrow S_0$) with a time constant of τ_f=12.1 nanoseconds (ns),[26] (ii) intersystem crossing to $|\nu)T_1$ and $|0)T_1$ in sequence ($|0)S_1 \rightsquigarrow |\nu)T_1 \rightsquigarrow |0)T_1$) with a composite time constant of τ_{ISC}=17.5 ns[26] or (iii) one-photon excitation to $|\nu)S_2$ ($|0)S_1 \rightarrow |\nu)S_2$). The isoenergetic internal conversion to S_0 caused by vibronic interactions is neglected because it is much slower than processes (i) and (ii).[26] The ClAlPc molecules promoted to $|\nu)S_2$, either by two-photon $S_0 \rightarrow |\nu)S_2$ excitation or one-photon $|0)S_1 \rightarrow |\nu)S_2$ excitation, non-radiatively relax to $|0)S_2$, $|\nu)S_1$ and $|0)S_1$ in sequence ($|\nu)S_2 \rightsquigarrow |0)S_2 \rightsquigarrow |\nu)S_1 \rightsquigarrow |0)S_1$) with an overall lifetime of τ_{S2}=900 femtoseconds (fs), which is determined by saturating the absorption of $|0)S_1$ state with a 18 ps laser pulse.[27] Afterward, they undergo one of the three processes mentioned above. The ClAlPc molecules relaxing to $|0)T_1$ by the intersystem-crossing relaxation $|0)S_1 \rightsquigarrow |\nu)T_1 \rightsquigarrow |0)T_1$ further experience another intersystem-crossing to S_0 ($|0)T_1 \rightsquigarrow S_0$) with a time constant of τ'_{ISC}=370 microseconds (μs).[28] Because τ_f (12.1 ns) and τ_{ISC} (17.5 ns) are much longer than τ (19 ps), we neglect $|0)S_1 \rightsquigarrow S_0$, $|0)S_1 \rightsquigarrow |\nu)T_1 \rightsquigarrow |0)T_1$ and $|0)T_1 \rightsquigarrow S_0$ relaxations, as well as $|0)T_1 \rightarrow |\nu)T_2$ excitation, in the course of pulse-matter interaction. Accordingly, the Beer′s law equation can be written as[29]

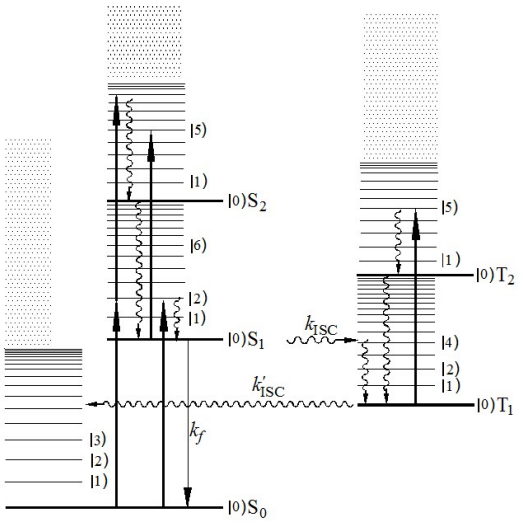

Fig. 3 Scheme of the five-energy-band model for ClAlPc/EtOH. Upward-pointing arrows denote optical excitation; wiggly lines denote non-radiative relaxation; and downward-pointing arrows denote radiative relaxation.

$$\frac{dI}{dz'} \equiv -\alpha I = -\left[\sigma_{S0}N_{S0} + \sigma_{S1}N_{S1}\right]\times I - \beta N_{S0}\times I^2 \quad (5)$$

in which the arguments (z',r,t) for I and N's are omitted. z' denotes the penetration depth of a pulse into the sample, t the time relative to the pulse peak, α the overall absorption coefficient, σ's the absorption cross sections of the states specified by the subscripts, β the two-photon absorption coefficient of S_0 and N's the ClAlPc concentrations of the states specified by the subscripts. The population-change rates of the states involved in eqn (5) are[29]

$$\frac{dN_{S0}}{dt} = -\frac{\sigma_{S0}N_{S0}I}{\hbar\omega} - \frac{\beta N_{S0}I^2}{2\hbar\omega}, \quad (6)$$

$$\frac{dN_{S1}}{dt} = \frac{\sigma_{S0}N_{S0}I}{\hbar\omega} - \frac{\sigma_{S1}N_{S1}I}{\hbar\omega} + \frac{N_{S2}}{\tau_{S2}} \quad (7)$$

and

$$\frac{dN_{S2}}{dt} = \frac{\beta N_{S0}I^2}{2\hbar\omega} + \frac{\sigma_{S1}N_{S1}I}{\hbar\omega} - \frac{N_{S2}}{\tau_{S2}} \quad (8)$$

in which the arguments (z',r,t) for I and N's are omitted. $\hbar$ denotes Planck's constant and equals 1.05×10^{-34} J·s, ω is the angular frequency of a laser pulse and equals 3.53×10^{15} s^{-1} (corresponding to λ=532 nm), and $\hbar\omega$ denotes the photon energy and equals 3.71×10^{-19} J. Each term on the right hand sides of eqn (6)-(8) denotes the rate of population redistribution caused by one of the following four processes: one-photon $S_0\rightarrow|\nu)S_1$ excitation, two-photon $S_0\rightarrow|\nu)S_2$ excitation, one-photon $|0)S_1\rightarrow|\nu)S_2$ excitation and $|\nu)S_2\rightsquigarrow|0)S_2\rightsquigarrow|\nu)S_1\rightsquigarrow|0)S_1$ relaxation.[29,30] Considering that the sub-ps time periods for the $|\nu)S_1\rightsquigarrow|0)S_1$ and $|\nu)S_2\rightsquigarrow|0)S_2$ relaxations are much shorter than the pulse width τ (19 ps), we ignore the population bottlenecks at $|\nu)S_1$ and $|\nu)S_2$.

When the longest relaxation time τ_{ISC} (370 μs) is considerably shorter than the shortest $\tau_{p\text{-}p}$ used in this study (0.1 s), all the ClAlPc molecules promoted to the excited states relax to S_0 before the next pulse arrives. Therefore, all the ClAlPc molecules reside on S_0 with $N_{S1}(z',r,-3\tau)=N_{S2}(z',r,-3\tau)=0$ when a pulse starts to interact with the solution. In the following, we ignore ClAlPc migration driven by previous pulses and thus consider that $N_{S0}(z',r,-3\tau)$ is spatially uniform throughout the whole solution and equals 4.2×10^{17} cm^{-3} or 1.2×10^{17} cm^{-3}.

It is shown in the **Supporting Information** (**SI**) that, using the above-mentioned N's($z',r,-3\tau$) as the initial conditions of eqn (6)-(8) and $I(z'=0,r,t)=I_z(r,t)$ given in eqn (1) as the initial condition of eqn (5), we can derive $I(z',r,t)$, $N_{S0}(z',r,t)$, $N_{S1}(z',r,t)$ and $N_{S2}(z',r,t)$ by alternately integrating dN's(z',r,t')/dt' (see eqn (6)-(8)) over t' from -3τ to t and $dI(z'',r,t)/dz''$ (see eqn (5)) over z'' from 0 mm to z'. Here, t falls in the range $[-3\tau, 3\tau]$ and z' falls in the range [0, L=1.0 mm].

By integrating $I(z'=L,r,t)$, the intensity at the sample's exit surface derived above, over t from -3τ to 3τ and then over the beam cross section, we obtain the transmitted pulse energy

$$\mathcal{E}_2 = \int_0^{\infty}\int_{-3\tau}^{3\tau} I\left(z'=L,r,t\right)\cdot dt\cdot 2\pi r dr \quad (9)$$

to be compared with the D2 reading (see Fig. 2(a)). Based on eqn (9), we have previously fit the Z-scan data of a methanolic solution of ClAlPc and obtained $\sigma_{S0}=2.2\times10^{-18}$ cm^2, $\sigma_{S1}=2.3\times10^{-17}$ cm^2 and $\beta=2.5\times10^{-28}$ cm^4/W,[29] On the other hand, by integrating $-dI(z',r,t')/dz'$ over t' from -3τ to $t\leq3\tau$, we obtain the pulse energy absorbed by ClAlPc molecules in a unit of volume in the time interval $[-3\tau, t]$

$$\Delta\mathcal{E}_p\left(z',r,t\right) = -\int_{-3\tau}^{t}\frac{dI\left(z',r,t'\right)}{dz'}dt'. \quad (10)$$

Because each individual ClAlPc molecule in a dV does not necessarily absorb equal energy from a pulse, we cannot derive the pulse energy absorbed by individual ClAlPc molecules ($\Delta\varepsilon_p$) in the dV by simply dividing $\Delta\mathcal{E}_p(z',r,t)$ by the solute concentration $N_{S0}(z',r,-3\tau)$. Instead, we derive $\Delta\varepsilon_p$ by tracking the excitation and relaxation behaviours of individual ClAlPc molecules (in addition to alternately integrating eqn (5) and eqn (6)-(8) to evaluate $I(z',r,t)$, $N_{S0}(z',r,t)$, $N_{S1}(z',r,t)$ and $N_{S2}(z',r,t)$). As shown in the **SI**, by counting the numbers of one-photon $S_0\rightarrow|\nu)S_1$, two-photon $S_0\rightarrow|\nu)S_2$ and one-photon $|0)S_1\rightarrow|\nu)S_2$ excitation processes that individual ClAlPc molecules on $|0)S_1$ and $|0)S_2$ have experienced up to $t\leq3\tau$, we decompose $N_{S1}(z',r,t)$ and $N_{S2}(z',r,t)$ into their components $N_{ES1}(i;z',r,t)$ and $N_{ES2}(i;z',r,t)$ which designate the concentrations of ClAlPc molecules on $|0)S_1$ and $|0)S_2$ that have absorbed i photons ($i\geq1$) up to t. $N_{ES1}(i;z',r,t)+N_{ES2}(i;z',r,t)$, denoted by $N_E(i;z',r,t)$ henceforth, designates the concentrations of ClAlPc molecules on S_0, $|0)S_1$ or $|0)S_2$ (all the ClAlPc molecules indeed) that have absorbed i photons ($i\geq1$) individually, with energy of $i\hbar\omega$, up to t. Because τ_f (12.1 ns) is much longer than τ (19 ps), ClAlPc molecules on $|0)S_1$ do not undergo $|0)S_1\rightsquigarrow S_0$ relaxation during the pulse-matter interaction. This means that $N_{S0}(z',r,t)$ does not contribute to $N_E(i;z',r,t)$ for $i\geq1$.

By further counting the numbers of $|\nu)S_1\rightsquigarrow|0)S_1$ and $|\nu)S_2\rightsquigarrow|0)S_2\rightsquigarrow|\nu)S_1\rightsquigarrow|0)S_1$ relaxation processes that individual ClAlPc molecules have experienced up to $t\leq3\tau$, we can derive $\Delta\varepsilon_e$ converted from $\Delta\varepsilon_p$. Specifically, each $|\nu)S_1\rightsquigarrow|0)S_1$ relaxation process subsequent to the $S_0\rightarrow|\nu)S_1$ excitation drives the conversion of $\hbar(\omega-\omega_{S1})$ from $\Delta\varepsilon_p$ into $\Delta\varepsilon_e$ in individual ClAlPc molecules. Here ω_{S1} corresponds to the energy of $|0)S_1$ relative to S_0 and hence a wavelength of 673 nm.[29] Each $|\nu)S_2\rightsquigarrow|0)S_2\rightsquigarrow|\nu)S_1\rightsquigarrow|0)S_1$ relaxation process subsequent to the one-photon $|0)S_1\rightarrow|\nu)S_2$ excitation drives the conversion of $\hbar\omega$ from $\Delta\varepsilon_p$ into $\Delta\varepsilon_e$ in individual ClAlPc molecules. Besides, each $|\nu)S_2\rightsquigarrow|0)S_2\rightsquigarrow|\nu)S_1\rightsquigarrow|0)S_1$ relaxation process subsequent to the two-photon $S_0\rightarrow|\nu)S_2$ excitation drives the conversion of $(2\hbar\omega-\omega_{S1})$ from $\Delta\varepsilon_p$ into $\Delta\varepsilon_e$ in individual ClAlPc molecules. Here we disregard the insignificant $\Delta\varepsilon_p$ into $\Delta\varepsilon_e$ conversion driven by the long lasting $|0)S_1\rightsquigarrow S_0$, $|0)S_1\rightsquigarrow|\nu)T_1\rightsquigarrow|0)T_1$ and $|0)T_1\rightsquigarrow S_0$ relaxation processes.

Because τ_{S2} (900 fs) is considerably shorter than τ (19 ps) and τ_f (12.1 ns) is much longer than τ, individual ClAlPc molecules undergo the $|0)S_1\rightarrow|\nu)S_2$ excitation process several times and the other two excitation processes 0 or 1 time. Hence, it is plausible that $\Delta\varepsilon_p$ is predominantly driven by $|0)S_1\rightarrow|\nu)S_2$ excitation and the $\Delta\varepsilon_p$ into $\Delta\varepsilon_e$ conversion is overwhelmingly propelled by the subsequent $|\nu)S_2\rightsquigarrow|0)S_2\rightsquigarrow|\nu)S_1\rightsquigarrow|0)S_1$ relaxation. Both the excitation and relaxation processes repeat equal times alternately during the pulse-matter interaction. Accordingly, $\Delta\varepsilon_p$ nearly equals ε_e.

Because τ (19 ps) is comparable with the inter-molecular excess energy transfer time (13 ps, *vide infra*) and considerably longer than the time for intra-molecular $\Delta\varepsilon_p$ into $\Delta\varepsilon_e$ conversion (τ_{S2}= 900 fs), the intra- and inter-molecular relaxation processes are readily separable in time. Accordingly, $\Delta\varepsilon_e$ retained in individual ClAlPc molecules nearly equals $\Delta\varepsilon_p$ at any time $t\leq3\tau$ and reaches its maximum at $t=3\tau$ at which $\Delta\varepsilon_e$ of individual EtOH molecules nearly equals 0. With $\Delta\varepsilon_p$ and $\Delta\varepsilon_e$ derived for any $t\leq3\tau$, we can further deduce $\Delta\varepsilon_t=f\times\Delta\varepsilon_p$ for $t\leq3\tau$ where f denotes the fraction of $\Delta\varepsilon_e$ (~$\Delta\varepsilon_p$) converted into $\Delta\varepsilon_t$.

When numerically evaluating $\Delta\varepsilon_p$ for $t\leq3\tau$ in the **SI**, we slice the sample into 10 layers and divide each pulse into 5000 temporal segments. Accordingly, each layer of the sample has a thickness of $\Delta z'$=0.1 mm and each temporal segment of a pulse has a width of $\Delta t=6\tau/5000$=22.8 fs.

Using $\sigma_{S0}=2.2\times10^{-18}$ cm^2, $\sigma_{S1}=2.3\times10^{-17}$ cm^2 and $\beta=2.5\times10^{-28}$ cm^4/W, we solve eqn (S.5)-(S.7) in the **SI** at the desired z, z' and r to evaluate $N_{S0}(z',r,t)$, $N_{S1}(z',r,t)$ and $N_{S2}(z',r,t)$ for $t\leq3\tau$, from which we

derive $N_{ES1}(i;z',r,3\tau)$ with $i \geq 1$ and $N_{ES2}(i;z',r,3\tau)$ with $i \geq 2$. Note that the fact that individual ClAlPc molecules on $|0)S_2$ absorb at least two photons demands that $i \geq 2$ in $N_{ES2}(i;z',r,3\tau)$. For simplicity, we drop the arguments z', r or t of $I(z',r,t)$, $N_{S0}(z',r,t)$, $N_{S1}(z',r,t)$, $N_{S2}(z',r,t)$, $N_{ES1}(i;z',r,t)$, $N_{ES2}(i;z',r,t)$, $N_E(i;z',r,t)$, etc., fully or partially, in the following unless it is necessary to express them explicitly. Fig. 4 shows $N_E(i;z',r,3\tau)$ at z=0, z'=0.1, 0.5 and 1.0 mm, respectively, and r=0 as a function of i in three frames. Each frame is for a specific z' and contains six curves: circles, hollow triangles and hollow asterisks corresponding to $\mathcal{E}_1$=8.7, 4.5, and 1.1 μJ, respectively, and $N_{S0}(-3\tau)$= 4.2×10^{17} cm^{-3}, as well as dots, solid triangles and solid asterisks corresponding to $\mathcal{E}_1$=8.7, 4.5 and 1.1 μJ, respectively, and $N_{S0}(-3\tau)=1.2\times10^{17}$ cm^{-3}. By comparing the dots with the circles in each frame, we note that the dots peak at the same absorbed photon number i (35) as the circles in frame (a) but peak at a larger i (33 and 32) than the circles (31 and 28) in frames (b) and (c), respectively. Similarly, the same trend is found between the solid triangles and the hollow triangles as well as the solid asterisks and the hollow asterisks. This indicates that individual ClAlPc molecules, except for those in the first layer (z'=0.1 mm), in the dilute solution tend to absorb more pulse energy $\Delta\mathcal{E}_p$ and hence carry more translational energy $\mathcal{E}_t$ ($\mathcal{E}_{t0}+\Delta\mathcal{E}_t$, with $\Delta\mathcal{E}_t=f\times\Delta\mathcal{E}_p$) after intra-molecular $\Delta\mathcal{E}_e$ into $\Delta\mathcal{E}_t$ conversion ends at $t=3\tau$, at which the inter-molecular excess energy transfer is not apparent yet. Because each curve in Fig. 4 covers a range of i considerably larger than 1 or 2 (absorbed photon numbers pertaining to one-photon $S_0\rightarrow|\nu)S_1$ excitation or two-photon $S_0\rightarrow|\nu)S_2$ excitation that individual ClAlPc molecules experience during the pulse-matter interaction), $\Delta\mathcal{E}_p$ is predominantly driven by repetitive $|0)S_1\rightarrow|\nu)S_2$ excitation interspersed with $|\nu)S_2\rightsquigarrow|0)S_2\rightsquigarrow|\nu)S_1\rightsquigarrow|0)S_1$ relaxation which fully converts $\Delta\mathcal{E}_p$ into $\Delta\mathcal{E}_e$.

After the pulse excitation and intra-molecular relaxation ends at $t=3\tau$, the inter-molecular excess energy transfer process carries on to bring the excited ClAlPc/EtOH to local thermodynamic equilibrium at $t=\tau_{therm}$. Here τ_{therm} denotes the local thermal equilibrium time, the time for the excited solution to restore local thermal equilibrium by successive inter-molecular excess energy transfer subsequent to the intra-molecular relaxation. Taking the energy transfer time to be that from an azulene molecule to the surrounding methanol molecules, experimentally determined to be 13 ps by Seilmeier and Kaiser,[25] we estimate τ_{therm} to be 187 ps and 283 ps for the concentrated and dilute solutions, respectively, according to Ref.[30]. After t reaches τ_{therm}, $\Delta\mathcal{E}_t$ is nearly equal for individual molecules of both ClAlPc and EtOH in the same dV. However, it is much smaller than that associated with individual ClAlPc molecules at $t=3\tau$. At this stage ($t=\tau_{therm}$), the temperature θ becomes definable and is proportional to $<\mathcal{E}_t>$ with $\mathcal{E}_t=\mathcal{E}_{t0}+\Delta\mathcal{E}_t$.

After $N_E(i;z',r,3\tau)$ is derived in the **SI** and plotted as a function of i in Fig. 4, we proceed to simulate $\Delta\theta$ ($\propto<\Delta\mathcal{E}_t>$) pertaining to the excited ClAlPc/EtOH restoring local thermal equilibrium

$$\Delta\theta(z',r)=\frac{\sum_{i=1}^{2501}N_E(i;z',r,3\tau)\times i\hbar\omega}{\rho c_p}. \quad (11)$$

The numerator denotes the sum of $\Delta\mathcal{E}_p$ for $t=3\tau$ over all the excited ClAlPc molecules contained in a unit of volume. This energy, equal to $\Delta\mathcal{E}_p(z',r,3\tau)$ derived from eqn (10), is nearly completely dissipated throughout the surrounding solvent molecules as heat in τ_{therm}. The denominator is the product of the solvent density ρ and isobaric specific heat c_p. Here, ρ equals 0.79 g/cm^3 and c_p equals 2.44 J/(g·K).[31]

Based on eqn (11), we calculate $\theta(\theta_0+\Delta\theta(z',r))$ as a function of r for z'=0.1, 0.5 and 1.0 mm, respectively, and z=0. Fig. 5 shows the results obtained with $\mathcal{E}_1$=8.7 μJ. Frames (a), (b) and (c) are for the first (z'=0.1 mm), middle (z'=0.5 mm) and last (z'=1.0 mm) layers of the sample at 4.2×10^{17} cm^{-3} (dashed-lines) and 1.2×10^{17} cm^{-3} (solid-lines). It is evident that the concentrated solution shows a higher

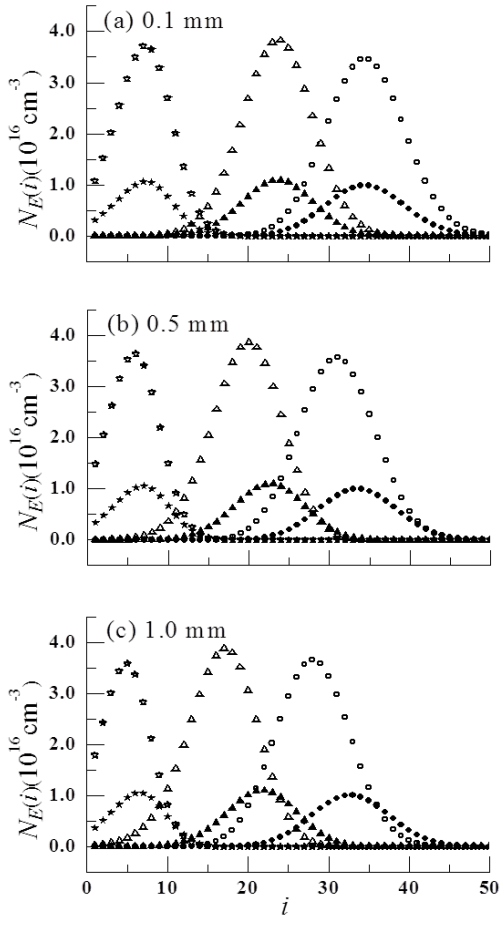

Fig. 4 Plots of $N_E(i;3\tau)$ at z=0 and r=0 as a function of i. Circles, hollow triangles and hollow asterisks correspond to $\mathcal{E}_1$=8.7, 4.5 and 1.1 μJ, respectively, and $N_{S0}(-3\tau)=4.2\times10^{17}$ cm^{-3}. Dots, solid triangles and solid asterisks correspond to $\mathcal{E}_1$=8.7, 4.5, and 1.1 μJ, respectively, and $N_{S0}(-3\tau)=1.2\times10^{17}$ cm^{-3}. Frames (a), (b) and (c) correspond to 3 penetration depths, z'=0.1, 0.5 and 1.0 mm, respectively.

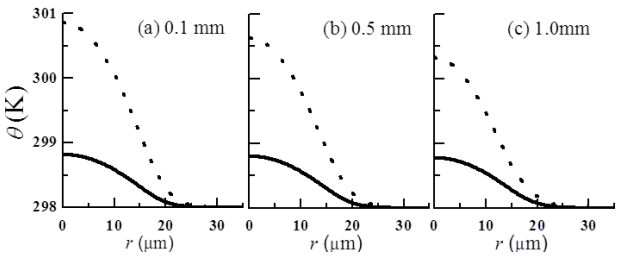

Fig. 5 Plots of θ, simulated with $\mathcal{E}_1$=8.7 μJ at z=0, as a function of r. Frames (a), (b) and (c) pertain to 3 penetration depths, z'=0.1, 0.5 and 1.0 mm, respectively. The dashed-lines and solid-lines correspond to $N_{S0}(-3\tau)=4.2\times10^{17}$ cm^{-3} and 1.2×10^{17} cm^{-3}, respectively.

temperature $\theta(\propto<\varepsilon_t>)$ at each r and thus a larger temperature gradient ($\nabla\theta$) along the r direction. A similar calculation for different input pulse energy levels, 4.5 and 1.1 μJ, shows the same trend. This reveals that individual solute molecules in the concentrated solution tend to retain more translational excess energy $\Delta\varepsilon_t$ after the solution restores local thermal equilibrium at $t=\tau_{therm}$.

For continuous light irradiation, $\Delta\varepsilon_t$ increases with $t\geq\tau_{therm}$ and is nearly equal for individual molecules of both ClAlPc and EtOH in the same dV at any time $t\geq\tau_{therm}$. $\theta\propto<\varepsilon_t>$ and $\nabla\theta$ are both larger in the concentrated ClAlPc/EtOH than in the dilute one.

4. Results and discussion

In the following, we show our experimental results of solute migration induced in ClAlPc/EtOH by short pulses and continuous light.

Short-pulse-induced solute migration

Using the *Z*-scan technique with the TEM_{00} mode 19 ps pulses at 532 nm, we have previously verified that a short pulse can induce solute migration in the solution at 4.2×10^{17} cm^{-3}.[19,32] When the input pulse energy $\mathcal{E}_1$ is above a threshold $\mathcal{E}_T$, the *Z*-scan curves obtained using pulses with pulse-to-pulse separations $\tau_{p\text{-}p}$'s shorter than τ_{md}=0.3 s skew upward toward the side scanned after the beam waist (the +*z* side). In addition, they appear higher in the vicinity of the beam waist than the symmetrical curves obtained with pulses of equal energy and $\tau_{p\text{-}p}$'s considerably longer than τ_{md}. In contrast, when $\mathcal{E}_1$ is below $\mathcal{E}_T$, the *Z*-scan curves are $\tau_{p\text{-}p}$ independent and appear symmetrical about the beam waist. Accordingly, we attributed the skewness of the curves obtained with $\mathcal{E}_1>\mathcal{E}_T$ and $\tau_{p\text{-}p}<\tau_{md}$ to absorption weakening by the outward solute migration, an accumulative effect sustained across neighbouring pulses. In addition, we explained the threshold energy $\mathcal{E}_T$ as a result of potential well entrapment of solute molecules formed by the attractive forces of neighbouring solvent molecules (see Fig. 1). Only when $\mathcal{E}_1$ exceeds $\mathcal{E}_T$ do some of the solute molecules gain sufficient translational excess energy ($\Delta\varepsilon_t>-\mu-\varepsilon_{t0}$) to escape from the entrapment and hop along a zigzag trajectory, causing jumps interspersed with oscillations within different wells, namely, movement. When individual solute molecules at the beam center tend to gain more $\Delta\varepsilon_t$ than those at the periphery, the solution shows outward solute migration.

Fig. 6 shows the present *Z*-scan results of the solution at 4.2×10^{17} cm^{-3} and 1.2×10^{17} cm^{-3} in columns I and II, respectively. Each frame in both columns contains two curves obtained with pulses of the same input energy $\mathcal{E}_1$ and two τ_{p-p}'s. The dotted and crossed curves denote the data taken with τ_{p-p}=0.1 and 1.0 s, respectively. In frames (a) of columns I and II, both the dotted and crossed curves are indistinguishable and symmetrical about the beam waist at z=0. This feature excludes the outward-solute-migration-induced absorption weakening, indicating that $\mathcal{E}_1$=1.1 μJ is insufficient to induce the outward solute migration in the solution at both concentrations. Otherwise, the dotted curves skew upward toward the +*z* side and appear higher than the crossed ones in the vicinity of the beam waist. The appearance of the valleys at the beam waist categorizes the sample absorption as reverse saturable absorption (RSA) due to individual pulse effects. RSA refers to a situation in which α increases with the intensity $I(t)$ or the generalized fluence $F_G(t)$ ($\equiv\int_{-\infty}^{t}I(t')dt'$) of a pulse. RSA due to individual pulse effects signifies $\sigma_{S1}>\sigma_{S0}$, as explained in detail in Ref.[19]. When $\mathcal{E}_1$ is increased to 4.5 μJ, the dotted and crossed curves in frame (b) of column I are nearly indistinguishable and symmetrical about the beam waist except for a minute asymmetrical deviation around z=0 for the dotted curve. This indicates that outward solute migration can barely be induced by a 4.5 μJ/19 ps pulse in the concentrated solution. In contrast, the curves in frame (b) of column II are noticeably split around z=0: the dotted one skews upward toward the +*z* side and appears significantly higher than the crossed one, symmetrical about the beam waist. This discrepancy indicates that a 4.5 μJ/19 ps pulse induces, in the vicinity of the beam waist, the outward solute migration in the dilute solution. Comparison between frames (b) of columns I and II reveals that the energy threshold $\mathcal{E}_T$ for the concentrated solution is higher or equal to 4.5 μJ, whereas $\mathcal{E}_T$ for the dilute solution is lower than 4.5 μJ. Accordingly, we infer that individual solute molecules in the dilute solution gain sufficient translational energy ε_t to exceed the potential well barrier $-\mu$ at $t\leq3\tau$ and those in the concentrated solution acquire ε_t insufficient to surpass $-\mu$ up to $t=3\tau$ (see the solid triangles and hollow triangles in Fig. 4).

Further increasing $\mathcal{E}_1$ to 8.7 μJ from 4.5 μJ, we find that the outward solute migration is first activated evidently in the concentrated solution, as judged from frames (b) and (c) of column I; however, the solute migration becomes more severe in the dilute solution, as shown by the comparison between frames (b) and (c) of column II. Accordingly, we infer that individual solute molecules in the concentrated solution obtain sufficient ε_t at $t\leq3\tau$ to exceed the potential well barrier $-\mu$ (see the dots and circles in Fig. 4) although this ε_t is smaller than that pertaining to individual solute molecules in the dilute solution.

Note that, at $\mathcal{E}_1$=4.5 μJ, the *NT* ratio of the dots to the crosses at z=0 for the concentrated solution is smaller than that for the dilute solution. Contrarily, at $\mathcal{E}_1$=8.7 μJ, it is larger than that for the dilute solution. This indicates that the concentrated solution shows less movement of individual solute molecules at $t\leq3\tau$ disregarding the input pulse energy; however, it exhibits less solute migration at $\mathcal{E}_1$=4.5 μJ but more solute migration at $\mathcal{E}_1$=8.7 μJ. This means that when $\mathcal{E}_1$ is increased to exceed $\mathcal{E}_T$ for the concentrated solution, the concentration of solute molecules participating in the solute migration is greatly increased.

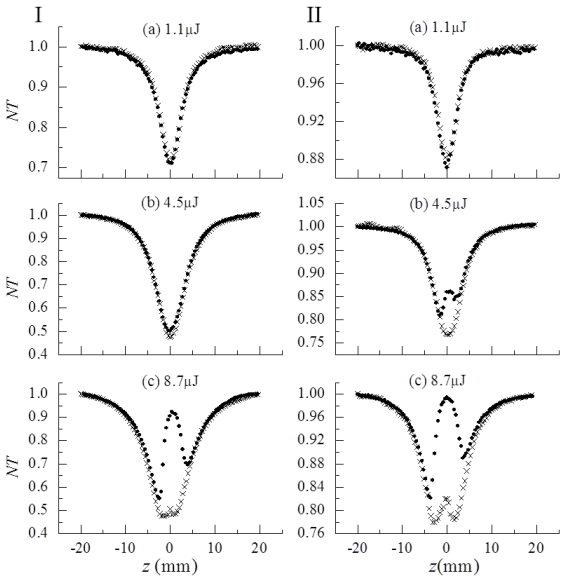

Fig. 6 *Z*-scan results of ClAlPc/EtOH with $N_{S0}(-3\tau)$= 4.2×10^{17} cm^{-3} (column I) and $N_{S0}(-3\tau)$=1.2×10^{17} cm^{-3} (column II). Dots and crosses denote τ_{p-p}=0.1 and 1.0 s, respectively. Frames (a), (b) and (c) pertain to $\mathcal{E}_1$=1.1, 4.5, and 8.7 μJ.

Because individual EtOH molecules stand still with $\varepsilon_t=\varepsilon_{t0}$ when the nearby individual solute molecules start to move, the potential well entrapment holds and causes a threshold energy $\mathcal{E}_T$ that a pulse

needs to surpass to induce the outward solute migration.

In contrast to the dilute solution, the concentrated one pertains to a lower linear transmittance and shows lower valleys in the *Z*-scan curves (compare the crossed curves in frames (a) and (b) of columns I and II). This indicates the solute molecules in the concentrated solution absorb more pulse energy collectively.[32]

Continuous-light-driven thermal diffusion

Using the transmittance measurement technique with the TEM_{00} mode CW HeNe laser at 2.5 mW, we have previously verified continuous-light-driven thermal diffusion in ClAlPc/EtOH at the concentration of 4.2×10^{17} cm^{-3}.[21] By plotting the transmittance T' as a function of t, we found that T' increases with t monotonically (see Fig. 5 and the associated inset in Ref.[21]: dots for experiment and solid curve for simulation). In the first ~50 μs after the shutter is opened at t=0, T' increases with t rapidly due to $S_0\rightarrow|\nu)S_1$, $|0)S_1\rightarrow|\nu)S_2$ and $|0)T_1\rightarrow|\nu)T_2$ excitations with $\sigma_{S0}>\sigma_{S1}$ and $\sigma_{S0}>\sigma_{T1}$, a sign of saturable absorption (SA).[21] Note that because 50 μs is much longer than τ_{SC}=17.5 ns, $|0)T_1\rightarrow|\nu)T_2$ excitation can no longer be ignored, as in the case of 19 ps pulse excitation. After t exceeds ~50 μs, the increase of T' with t becomes slower gradually and stationary eventually on the time scale of mass diffusion (τ_{md}=0.3 s). This is because $\nabla\theta$-driven outward solute migration, i.e., thermal diffusion, becomes more significant as time goes on and is then gradually balanced by the mass diffusion. If the thermal diffusion did not come into play, T' would follow the dashed curve simulated with thermal diffusion and mass diffusion ignored.

Fig. 7 shows the present transmittance measurements of the solution at 4.2×10^{17} cm^{-3} and 1.2×10^{17} cm^{-3}. Frames (a) and (b) show T' as a function of t for the concentrated and dilute solutions, respectively. Each of these two frames contains two curves: the dotted one in (a) and the crossed one in (b) are the experimental results, and the dashed ones in (a) and (b) are the simulation results with both the thermal diffusion and mass diffusion ignored. Because the solute molecules in the concentrated solution absorb more photo energy collectively via $S_0\rightarrow|\nu)S_1$, $|0)S_1\rightarrow|\nu)S_2$ and $|0)T_1\rightarrow|\nu)T_2$ excitation, the dotted curve in frame (a) shows lower transmittance T' than the crossed one in frame (b). Frame (c) shows the dotted and crossed curves in frames (a) and (b), both normalized to T' at t ~50 μs, at which rapid transmittance increase stops. The fact that the dotted curve appears higher than the crossed one indicates that individual ClAlPc (and EtOH) molecules in the concentrated solution possess more $\mathcal{E}_t$ and thus show more movement which causes more solute migration at $t\geq\tau_{therm}$. This solute migration is a quasistatic process, referred to as thermal diffusion. As was explained in the **Introduction** section, the driving force for solute migration is proportional to $\nabla\theta$ ($\propto\nabla<\mathcal{E}_t>$) which is larger in the concentrated solution (see Fig. 5).

In summary, we experimentally verified that, for short pulse excitation, the concentrated ClAlPc/EtOH shows stronger absorption but more/less solute migration depending on the pulse energy; for continuous light irradiation, it always shows stronger absorption and more solute migration regardless of the light power. By theoretically certifying that solute molecules in the concentrated solution, compared to those in the dilute one, absorb more photo energy collectively and less photo energy individually, we consider the solute migration as net movement of individual solute molecules. By simulating movement of individual solute molecules and then summing up movement of individual solute molecules in a unit of volume, we deduce the solute migration behaviours which coincide with the experimental results. In our theoretical deduction, the short-pulse-induced and continuous-light-driven solute migrations differ in that the intra- and inter-molecular relaxation processes are readily separable for 19 ps pulse excitation but inseparable for continuous light irradiation.

Besides clarifying the short-pulse-induced and continuous-light-driven solute migrations in ClAlPc/EtOH, we also verify how its absorption properties vary with the pulse width and wavelength together: RSA for 532 nm 19 ps laser pulses and SA for 632.8 nm continuous laser light. In the future, we will conduct the same measurements using both short pulses and continuous light at 532 nm and/or 632.8 nm. This will help us to know how the absorption properties vary with pulse width and/or wavelength independently.

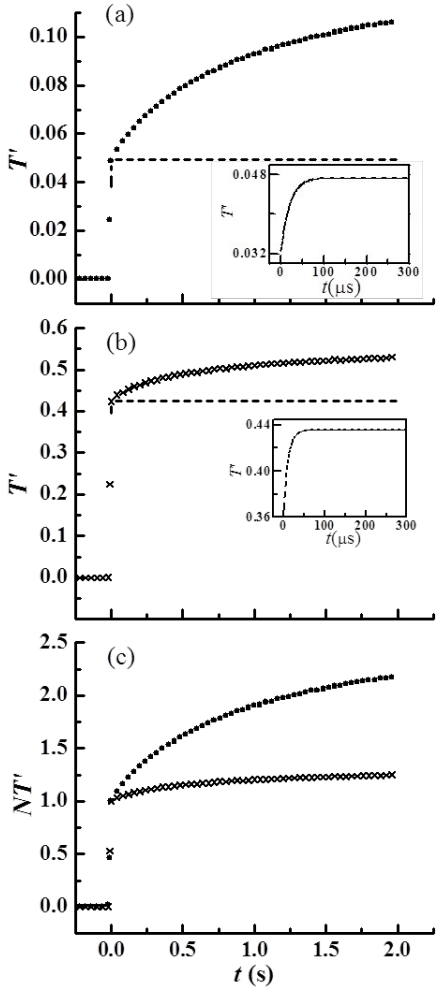

Fig. 7 (a-b) Plots of T's as a function of t for ClAlPc/EtOH with $N_{S0}(-3\tau)=4.2\times10^{17}$ cm^{-3} and 1.2×10^{17} cm^{-3}, respectively. The dotted curve in (a) and the crossed curve in (b) are experimental results. The dashed curves are simulation results with both thermal and mass diffusions ignored. (c) Plots of NT's as a function of t. The dotted and crossed curves are normalized from the ones shown by the same symbols in (a) and (b). The insets in (a) and (b) show the blow-ups of the dashed curves for t<300 μs.

5. Conclusions

Ever since thermal diffusion was first found in a sodium-sulfate solution by Ludwig in 1856 and in other electrolyte solutions by Soret in 1879, it has been referred to as the Ludwig-Soret effect to commemorate their pioneering work.[33] Several attempts have been made to relate thermal diffusion to parameters such as molecular potentials, partial molar enthalpies, and energy barriers;[34–37] however, a physical explanation of thermal diffusion at the molecular level is

not yet clear to date.[38,39] In this study, we have extensively discussed the microscopic view of the photo-absorption-caused solute migration (including thermal diffusion). In the future, we will further tackle how the solvent molecules pick up excess energy from the solute molecules excited by short pulses or continuous light and then carry out molecular migration. This will assuredly help the understanding of photo-absorption-caused migration of molecules of different components at the microscopic level.

Acknowledgements

The authors would like to thank the National Science Council of Taiwan for financially supporting this research under T. H. W. (NSC 102-2112-M-194-002-MY3) and C. I. L. (MOST 104-2113-M-194-006).

Notes and references

1 P. W. Atkins, *Physical Chemistry*, 7th ed. Oxford University Press, Oxford, 2002, p. 705.

2 K. Stowe, *Introduction to Statistical Mechanics and Thermodynamics*, John Wiley & Sons, Inc., New York, 1984, Ch. 5.

3 D. Landau, and E. M. Lifshitz, *Course of Theoretical Physics. Vol. 6 Fluid Mechanics*, 2nd ed. Pergmin Press, New York, 1987, Ch. 6.

4 S. R. de Groot and P. Mazur, *Non-Equilibrium thermodynamics*, Dover publications, Inc. New York, 1962, Ch. 11.

5 J. V. Sengers and J. M. Ortiz de Z´arate, in *Thermal Nonequilibrium Phenomena in Fluid Mixtures*, ed. W. Köhler, and S. Wiegand, Springer Berlin, Heidelberg, 2002, p. 121.

6 T. Elperin, N. Kleeorin, and I. I. Rogachevskii, Turbulent Thermal Diffusion of Small Inertial Particles. *Phys. Rev. Lett.*, 1996, **76**, 224.

7 A. H. Emery, and H. G. Drickamer, Thermal Diffusion in Polymer Solutions, *J. Chem. Phys.*, 1955, **23**, 2252.

8 K. J. Zhang, M.E. Briggs, R.W. Gammon, and J.V. Sengers, Thermal and mass diffusion in a semidilute good solvent-polymer solution, *J. Chem. Phys.*, 1999, **111**, 2270.

9 J. K. G. Dhont, S. Wiegand, S. Dhur, and D. Braun, Thermodiffusion of Charged Colloids: Single-Particle Diffusion, *Langmuir*, 2007, **23**, 1674.

10 N. V. Tabiryan, and W. Luo, Soret feedback in thermal diffusion of suspensions, *Phys. Rev. E*, 1998, **57**, 4431.

11 H. Löwen, Colloidal soft matter under external control, *J. Phys.: Condens. Matter*, 2001, **13**, R415.

12 S. A. Putnam, D. G. Cahill, and G. C. Wong, Temperature Dependence of Thermodiffusion in Aqueous Suspensions of Charged Nanoparticles, *Langmuir*, 2007, **23**, 9221.

13 Z. Wang, H. Kriegs, and S. Wiegand, Thermal Diffusion of Nucleotides, *J. Phys. Chem. B*, 2012, **116**, 7463.

14 S. R. Nersisyan, and N. V. Tabiryan, Space-time dynamics of nanoparticles of a magnetofluid in a laser beam, *J. Exp. Theor. Phys. Lett.*, 1998, **68**, 622.

15 W. Luo, and T. Du, Intensity dependent transmission dynamics in magnetic fluids, *J. App. Phys.*, 1999, **85**, 5953.

16 W. Luo, T. Du, and J. Huang, Novel Convective Instabilities in a Magnetic Fluid, *Phy. Rev. Lett.*, 1999, **82**, 4134.

17 M. Jerabek-Willemsen, C. J. Wienken, D. Braun, P. Baaske, and S. Duhr, Molecular Interaction Studies Using Microscale Thermophoresis, *Assay. Drug. Dev. Technol.*, 2011, **9**, 342.

18 M. Sheik-Bahae, A. A. Said, T. H. Wei, D. J. Hagan, and E. W. Van Stryland, Sensitive Measurement of Optical Nonlinearities Using a Single Beam, *IEEE J. Quantum Electron.*, 1990, **26**, 760.

19 T. H. Wei, C. C. Wang, T. T. Wu, C. W. Chen, X. B. Li, T. H. Huang, S. Yang, and T. Y. Wei, Mass transport following impulsive optical excitation, *J. Chem. Phys.*, 2004, **120**, 8031.

20 A. Yariv, *Optical Electronics*, Saunders, Chicago, 1991, p. 48.

21 L. S. Lee, C. I. Lee, P. C. Tsai, Y. C. Li, J. L. Tang, T. H. Wei, Thermal diffusion and convection induced in chloroaluminum phthalocyanine-ethanol by a CW He-Ne laser, *Chem. Phys. Lett.*, 2013, **558**, 93.

22 L. W. Hillman, *Dye Laser Principles*, Academic, New York, 1990, p. 27.

23 A. M. Schaffer, M. Gouterman, and E. R. Davidson, Porphyrins XXVIII. Extended Hückel calculations on metal phthalocyanines and tetrazaporphins, *Theor. chim. acta.*, 1973, **30**, 9.

24 T. H. Wei, T. H. Huang, and T. C. Wen, Mechanism of reverse saturable absorption in chloro-aluminum phthalocyanine solution studied with *Z*-scan, *Chem. Phys. Lett.*, 1999, **314**, 403.

25 A. Seilmeier, and W. Kaiser, in *Ultrashort Laser Pulses Generation and Applications*, ed. W. Kaiser, Springer-Verlag, Berlin, 1993, Ch. 7.

26 J. H. Brannon, and D. Madge, Picosecond Laser Photophysics. Group 3A Phthalocyanines, J. Am. Chem. Soc., 1980, **102**, 62.

27 T. H. Wei, T. H. Huang, H. D. Lin, and S.H. Lin. Lifetime determination for high-lying excited states using *Z* scan, *Appl. Phys. Lett*., 1995, **67**, 2266.

28 J. W. Perry, L. R. Khundkar, D. R. Coulter, D. Alvarez Jr., S. R. Marder, T. H. Wei, M. J. Sence, E. W. Van Stryland, and D. J. Hagan, in *Organic Molecules for Nonlinear Optics and Photonics, NATO ASI Series E*, ed. J. Messier, F. Kajzar, and P. Prasad, Kluwer Academic Publishers, Dordrecht, 1991, p. 369.

29 T. H. Wei, T. H. Huang, and J. K. Hu, Electronic energy dissipation in chloro-aluminum phthalocyanine/methanol system following nonlinear interaction with a train of picosecond pulses, *J. Chem. Phys.*, 2002, **116**, 2536.

30 T. H. Wei, T. H. Huang, and M. S. Lin, Signs of nonlinear refraction in chloroaluminum phthalocyanine solution, *Appl. Phys. Lett.*, 1998, **72**, 2505.

31 *CRC Handbook of Chemistry and Physics*, ed. D. R. Lide, CRC Press, Boca Raton, 76th edn, 1995. p.**15**-16.

32 C. K. Chang, Y. C. Li, C. W. Chen, L. S. Lee, J. L. Tang, C. C. Wang, C. C. Leu, T. H. Wei, T. H. Huang, and Y. L. Song, Solute migration caused by excited state absorptions, *J. Chem. Phys.*, 2009, **130**, 024511.

33 D. Reith, and F. Muller-Plathe, On the nature of thermal diffusion in binary Lennard-Jones liquids, *J. Chem. Phys.*, 2000, **112**, 2436.

34 L. J. T. M. Kempers, A comprehensive thermodynamic theory of the Soret effect in a multicomponent gas, liquid, or solid, *J. Chem. Phys.*, 2001, **115**, 6330.

35 S. R. de Groot, C. J. Gorter and W. Hoogenstraaten, La Méthode Thermo-Gravitationnelle De Séparation Appliquée Au Cas D'une Solution Aqueuse, *Physica*, 1943, **10**, 81.
36 R. Haase, H. W. Borgmann, K. H. Ducker, and W. P. Lee, Thermodiffusion im kritischen Verdampfungsgebiet binärer Systeme, *Z. Naturforsch. A*, 1971, **26**, 1224.
37 I. Prigogine, L. De Brouckere, and R. Amand, Recherches Sur La Thermodiffusion En Phase Liquide: (Première communication), *Physica*, 1950, **16**, 577.
38 C. Nieto-Draghi, J. B. Avalos, and B. Rousseau, Computing the Soret coefficient in aqueous mixtures using boundary driven nonequilibrium molecular dynamics, *J. Chem. Phys.*, 2005, **122**, 1.
39 C. N. Draghi, B. Rousseau, and J. B. Avalos. The Soret effect in aqueous solutions of associating fluids. Analysis of the anomalous change of sign with varying composition, *XII Congreso de Física Estadística*, Pamplona , 23-25 de octubre de 2003.